PHYSICAL REVIEW B **89**, 100101(R) (2014)

Inverse effect of morphotropic phase boundary on the magnetostriction of ferromagnetic $Tb_{1-x}Gd_xCo_2$

Chao Zhou,[1,*] Shuai Ren,[1,2] Huixin Bao,[1] Sen Yang,[1,†] Yonggang Yao,[1] Yuanchao Ji,[1] Xiaobing Ren,[1,2,‡]
Yoshitaka Matsushita,[3] Yoshio Katsuya,[3] Masahiko Tanaka,[3] and Keisuke Kobayashi[3]

[1]*Frontier Institute of Science and Technology, State Key Lab of Electrical Insulation and Power Equipment, MOE Key Laboratory for Nonequilibrium Synthesis and Modulation of Condensed Matter, School of Electrical Engineering, State Key Laboratory for Mechanical Behavior of Materials, Xi'an Jiaotong University, Xi'an 710049, China*

[2]*Ferroic Physics Group, National Institute for Materials Science, Tsukuba 305-0047, Ibaraki, Japan*

[3]*National Institute for Materials Science, Beamline BL15XU, Spring-8, 1-1-1 Kohto, Sayo-cho, Hyogo 679-5148, Japan*

(Received 8 December 2013; revised manuscript received 20 February 2014; published 4 March 2014)

The morphotropic phase boundary (MPB) has been utilized extensively in ferroelectrics and recently has attracted interest in ferromagnets [S. Yang, H. Bao, C. Zhou, Y. Wang, X. Ren, Y. Matsushita, Y. Katsuya, M. Tanaka, K. Kobayashi, X. Song, and J. Gao, Phys. Rev. Lett. **104**, 197201 (2010); R. Bergstrom, M. Wuttig, J. Cullen, P. Zavalij, R. Briber, C. Dennis, V. O. Garlea, and M. Laver, *ibid.* **111**, 017203 (2013)] for obtaining enhanced large field-induced strain. Here we report that the MPB can also lead to weakening (the inverse effect as compared to the known MPB materials) of field-induced strain, as exhibited in the $Tb_{1-x}Gd_xCo_2$ system. With synchrotron x-ray diffractometry, the structure symmetry of $TbCo_2$-rich compositions is detected to be rhombohedral below T_C and that of $GdCo_2$-rich compositions is tetragonal. The MPB composition $Tb_{0.1}Gd_{0.9}Co_2$, corresponding to the two phases (rhombohedral and tetragonal) of coexistence, shows the exotic minimum (near zero) magnetostriction as well as the largest magnetic susceptibility among all samples. Further analysis suggests that whether MPB can enhance or weaken magnetostriction is determined by the degree of magnetic ordering of two end members that form ferromagnetic MPBs, which was not considered previously. Our work not only reveals a new type of ferromagnetic MPB, but also provides a new recipe for designing functional high-susceptibility and low-strain magnetic materials.

DOI: 10.1103/PhysRevB.89.100101 PACS number(s): 75.30.Kz, 75.80.+q

Being physically parallel ferroic systems, ferromagnets and ferroelectrics are usually contrasted in functionalities and experimental phenomena [1,2]. In ferroelectrics, superior properties (e.g., high dielectric permittivity, large piezoelectricity, and large electrostriction) can be obtained by locating the material near a morphotropic phase boundary (MPB) [3–5], an ideally composition-induced phase transition boundary between the ferroelectric tetragonal (T) phase and ferroelectric rhombohedral (R) phase. At MPB, the system achieves a flattened free energy profile state which facilitates the polarization rotation and then yields a large piezoelectric response and electrostriction [4,6]. Because of such enhancement of properties at MPB, the MPB effects have attracted intense attention in ferroelectrics during the past decades [7–13].

Given the physical parallelism between ferroelectricity and ferromagnetism, it is of great interest to investigate the MPB phenomena in ferromagnets. Actually, it was already reported in the magnetostrictive $Tb_{1-x}Dy_xCo_2$ system [14], and its MPB composition shows enhanced large magnetostriction (dc-field response) and magnetic susceptibility (ac-field response) —similar to MPB phenomena of ferroelectrics.

The available results support that both ferroelectric and ferromagnetic MPBs can effectively enhance field-induced strain. Here in this work, we report a newly discovered ferromagnetic MPB system $Tb_{1-x}Gd_xCo_2$. Despite the similarity in the formula with the reported $Tb_{1-x}Dy_xCo_2$ and the same easy-domain-switching feature at MPB, $Tb_{1-x}Gd_xCo_2$ exhibits not enhanced but greatly weakened magnetostriction at MPB composition $Tb_{0.1}Gd_{0.9}Co_2$, showing the inverse effect of MPB as compared to the known MPB materials. The mechanism for this is discussed in detail later in this paper.

Following the MPB idea in ferroelectrics [6,15–18], we fabricated a pseudobinary ferromagnetic system with $TbCo_2$ (Ms//[111] below T_C) and $GdCo_2$ (Ms//[001] below T_C) [19,20]. The $Tb_{1-x}Gd_xCo_2$ alloy samples were prepared by arc melting method with the raw materials of Tb (99.9%), Gd (99.9%), and Co (99.9%) in an argon atmosphere. The synchrotron x-ray diffractometer (XRD) (with a strain resolution of about 5×10^{-4}) at the BL15XU NIMS beam line of Spring-8 was employed to determine the crystal symmetries. All the samples for synchrotron XRD were powders, and sealed into quartz capillaries with a diameter of 0.3 mm. The capillary was rotated during the measurement to reduce the preferred orientation effect and to average the intensity. The x-ray wavelength was 0.850 052 Ang. The samples used for the physical property measurements are polycrystalline. The magnetostriction was measured with strain gauges, and the magnetization (M) versus magnetic field (H) hysteresis loops were measured by using the vibrating sample magnetometer (VSM).

Figure 1(a) shows the composition-temperature phase diagram of $Tb_{1-x}Gd_xCo_2$ (abbreviated as xGd hereinafter), which was determined by the Curie temperature T_C detected from magnetization (M) versus temperature (T) curves [Fig. 1(b)] and the crystal structure [Figs. 1(c1) to 1(c4)] detected from the synchrotron XRD. Given the concurrence of the structural transition and ferromagnetic transition for ferromagnetic materials [21], the detected Curie temperature

*zhouch1982@gmail.com
†yang.sen@mail.xjtu.edu.cn
‡ren.xiaobing@mail.xjtu.edu.cn

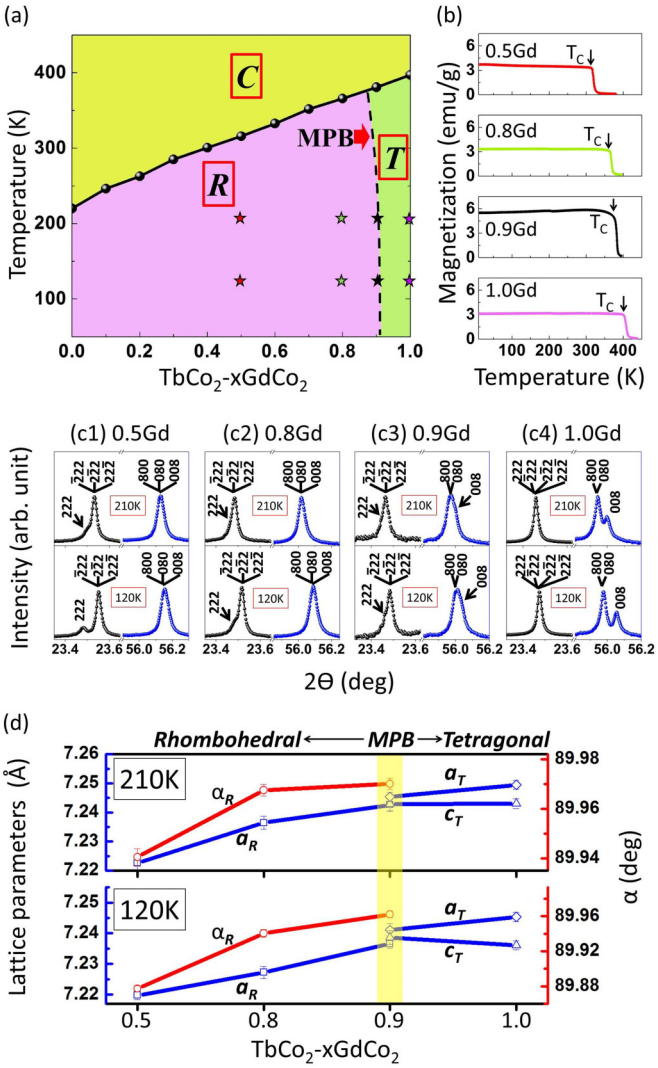

FIG. 1. (Color online) (a) Composition-temperature phase diagram of $Tb_{1-x}Gd_xCo_2$, in which C, R, and T denote cubic, rhombohedral, and tetragonal symmetries, respectively. (b) The magnetization (M) versus temperature (T) curves of 0.5, 0.8, 0.9, and 1.0 Gd (under 100 Oe). (c) The synchrotron x-ray diffraction patterns (typical 222 peaks and 800 peaks, with wavelength of 0.850 052 Ang) of (c1) 0.5, (c2) 0.8, (c3) 0.9, and (c4) 1.0 Gd. The five-star signals in Fig. 1(a) mark the sites of x-ray diffraction data in the phase diagram.

T_C also denotes the structural transition temperature. The surprising similarity (T-type phase boundaries) of $Tb_{1-x}Gd_xCo_2$ phase diagram to that of the $Tb_{1-x}Dy_xCo_2$ system [14], and ferroelectric MPB systems [3,6], indicates a universal existence of MPB in ferroic materials.

From the M-T curves [Fig. 1(b)], it is noted that with the increase of Gd concentration, T_C of $Tb_{1-x}Gd_xCo_2$ increases monotonously, while the magnetization (under 100 Oe) below T_C achieves maximum for 0.9Gd — about 5.5 emu/g and those of other compositions are all below 4.0 emu/g, indicating more fractions of domain switching in 0.9 Gd under a small field.

As for the XRD profiles, it is revealed that at 120 K, with increasing concentration of Gd, $Tb_{1-x}Gd_xCo_2$ exhibit a composition-induced crystallographic phase transition from R symmetry [bottom figure of Fig. 1(c1) for 0.5 Gd and bottom figure of Fig. 1(c2) for 0.8 Gd, with the characteristic splitting in the 222 peak but no splitting in the 800 peak] to T symmetry [bottom figure of Fig. 1(c4) for 1.0 Gd with the characteristic splitting in the 800 peak but no splitting in the 222 peak]. As for the XRD profile of 0.9 Gd [bottom figure of Fig. 1(c3)], it corresponds to the superposition of the R symmetry profile and T symmetry profile, similar to the MPB structure in the ferroelectric case [6]. The observed structural evolution at 120 K is consistent with the established relation between the easy axis direction and crystal structure [21]. And at higher temperature, such evolution is also observed from the XRD profiles of 0.5 Gd [210 K, top figure of Fig. 1(c1)], 0.8 Gd [210 K, top figure of Fig. 1(c2)], 0.9 Gd [210 K, top figure of Fig. 1(c3)], and 1.0 Gd [210 K, top figure of Fig. 1(c4)]. The calculated lattice parameters are shown in Fig. 1(d).

The structural evolution of $Tb_{1-x}Gd_xCo_2$ revealed by XRD profiles demonstrates the existence of MPB [denoted with a dashed line in Fig. 1(a)] in $Tb_{1-x}Gd_xCo_2$. It should be noted that near the T_C line of the phase diagram, the MPB boundary curves towards the left ($TbCo_2$ end member). This is predicted by the relation between the phase stability and Curie temperature, extracted from previously reported MPB-involved phase diagrams [2,3,6,14]. Among the available compositions 0.9 Gd is closest to MPB. Because both $TbCo_2$ and $GdCo_2$ possess cubic paramagnetic phase above T_C, a triple point of the C, R, and T phases naturally exists within the phase diagram, which is the key feature in ferroelectric MPB and also in ferromagnetic MPB [6,14,18].

Figure 2(a) shows the magnetization (M) versus magnetic field (H) loops for 0.5, 0.8, 0.9, and 1.0 Gd at 120 K under

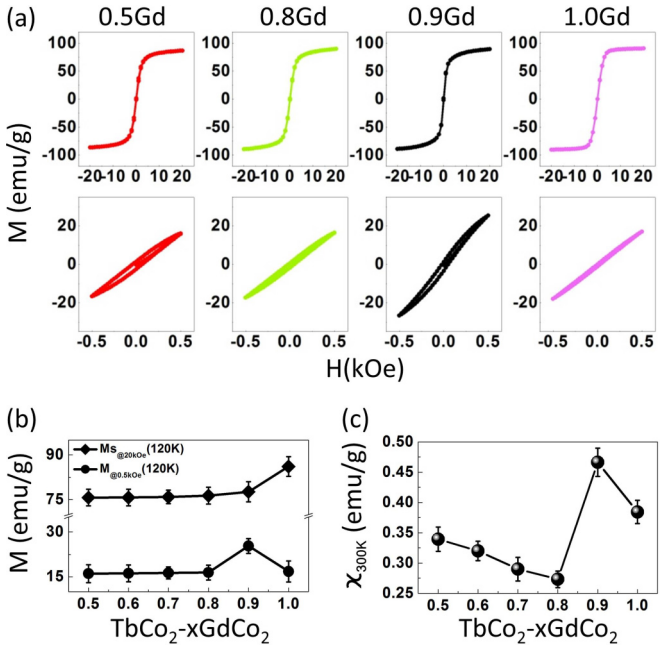

FIG. 2. (Color online) (a) The magnetization (M) versus magnetic field (H) hysteresis loops of 0.5, 0.8, 0.9, and 1.0 Gd under 20 and 0.5 kOe at 120 K. (b) The composition-dependent spontaneous magnetization under 20 kOe, and maximum magnetization under 0.5 kOe at 120 K. (c) The magnetic susceptibility of 0.5–1.0 Gd at 300 K.

20 and 0.5 kOe, respectively. The spontaneous magnetization (Ms) detected under 20 kOe increases monotonously with increasing Gd concentration, but the maximum magnetization exhibits an exotic peak value at 0.9 Gd under 0.5 kOe, as depicted in Fig. 2(b). The feature of easier domain switching reflected in Fig. 2 is consistent with that indicated in Fig. 1(b). At room temperature, the magnetic susceptibility of 0.9 Gd shows a peak value compared to off-MPB compositions [Fig. 2(c)]. Such a feature of easier domain switching has been regarded as the compensation of magnetic anisotropy in spin reorientation transition (SRT) [22,23]. Similar phenomena are also observed in ferroelectric MPB systems, and attributed to the weakening polarization (strain) anisotropy while approaching MPB [6,18,24,25].

Figure 3(a1) shows the magnetostriction curves of compositions 0.5, 0.8, 0.9, and 1.0 Gd. In the following, we focus the magnetostriction behaviors under small field (below 1 kOe) and large field (10 kOe), respectively.

(1) Interestingly, the change tendencies of magnetostriction curves under small field [below 1 kOe, purple-color shadowed in Fig. 3(a1)] for different samples exhibit two types of shapes: for 0.5 and 0.8 Gd, the magnetostriction curves exhibit a V shape, while for 1.0 Gd the magnetostriction curves exhibit a Λ shape. For the intermediate composition of 0.9 Gd, it shows a weak Λ-shaped curve and the minimum value of saturated magnetostriction among the available samples. The temperature-dependent magnetostriction results of 0.9 Gd under small field are shown in Fig. 3(a2) (purple-color-shadowed zone), and a similar phenomenon was observed—the shape of magnetostriction curves gradually change from Λ shaped at relative higher temperature (299.3 K) to V shaped at relatively lower temperature (36.4 K).

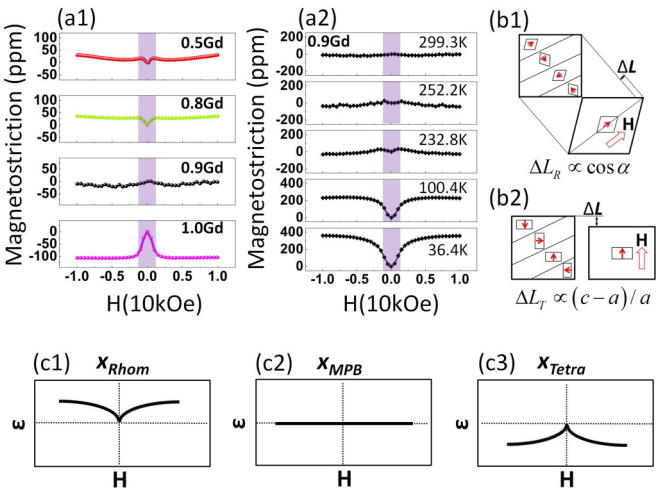

FIG. 3. (Color onloine) (a1) The magnetostriction curves (strain measurement direction and magnetic field direction are parallel) of 0.5, 0.8, 0.9, and 1.0 Gd at room temperature 299.3 K. (a2) The magnetostriction curves of 0.9 Gd at 299.3, 252.2, 232.8, 100.4, and 36.4 K. (b1, b2) The schematically mesoscopic explanations for anisotropic magnetostriction due to the switching of the noncubic ferromagnetic (=ferroelastic) domains for the two compounds, respectively, and the small rectangles and rhombuses represent the unit cell symmetry to be rhombohedral and tetragonal respectively. ΔL is the anisotropic magnetostriction due to magnetic field H. (c1–c3) The schematically symmetry-dependent magnetostriction curves under small field.

From the knowledge that ferromagnetic transition involves structure change, the anisotropic magnetostriction of the $Tb_{1-x}Gd_xCo_2$ system can be interpreted by the switching of noncubic ferroelastic domains, and the magnitude of magnetostriction is proportional to the size of the lattice distortion [21]. The XRD data in Fig. 1(d) indicates that the c/a ratio of $GdCo_2$ is less than unity. The negative saturation value of the magnetostriction of $GdCo_2$ [Fig. 3(a1)] reveals contraction behavior under an external field, consistent with the illustrated Λ-shaped magnetostriction curve in the T phase while c/a below 1 [Fig. 3(c3)], thus demonstrating the c direction of crystal aligns with the external field in the T phase as shown in Fig. 3(b2). For the crystal with R symmetry, it elongates along the field direction [Fig. 3(b1)] and exhibits a V-shaped curve as shown in Fig. 3(c1) [21]. Therefore, it is reasonably expected that at MPB, which is the phase boundary between the T and R phases, the magnetostriction behavior under small field exhibits neither V shape nor Λ shape, but a field-independent horizontal line [Fig. 3(c2)]. Furthermore, from the magnetostriction curves it is implied that the accurate MPB composition of $Tb_{1-x}Gd_xCo_2$ at room temperature is between 0.8 and 0.9 Gd. To generalize, the shape of the magnetostriction curves directly reflects the structural symmetry of ferromagnetic materials [21,26], and the magnetostriction measurement under small field can help determine where MPB accurately locates. The recently reported MPB system $Tb_{1-x}Dy_xCo_2$ exhibits a similar transformation around MPB [14].

(2) For MPB compositions of $Tb_{1-x}Dy_xCo_2$ and $Tb_{1-x}Gd_xCo_2$, despite their same magnetostrictive behavior under small field, they demonstrate different magnetostrictive behaviors under large field: $Tb_{0.3}Dy_{0.7}Co_2$ exhibits the largest magnetostriction while $Tb_{0.1}Gd_{0.9}Co_2$ exhibits the minimum magnetostriction. For the $Tb_{1-x}Dy_xCo_2$ system, compared to the T phase end member, its R phase end member corresponds to a higher magnetic ordering state—$TbCo_2$ with ⟨111⟩ symmetry possesses larger Ms than $DyCo_2$ with ⟨100⟩ symmetry [14]; for the $Tb_{1-x}Gd_xCo_2$ system, compared to the R phase end member, its T phase end member corresponds to a higher magnetic ordering state—the M-H measurement results show that $GdCo_2$ with ⟨100⟩ symmetry possesses larger Ms than $TbCo_2$ with ⟨111⟩ symmetry. Moreover, as for the two systems, the R phase end member $TbCo_2$ bears much larger lattice distortion than the T phase end members $DyCo_2$ and $GdCo_2$ [20,21,27]. Therefore, under large external magnetic field H, the MPB composition of $Tb_{1-x}Dy_xCo_2$ tends to transform to the R phase and exhibits large magnetostriction while the MPB composition of $Tb_{1-x}Gd_xCo_2$ tends to transform to a T phase and exhibits small magnetostriction, as Fig. 3 shows. In another famous ferromagnetic system cobalt ferrite, we have also discovered near-zero magnetostriction around MPB [28].

Considering the differences of the transitional behaviors of the two MPBs under external magnetic field H, $Tb_{1-x}Dy_xCo_2$ (also the famous Terfenol-D) is classified into type-I ferromagnetic MPB (type I FM MPB) as shown in Fig. 4(a1), and $Tb_{1-x}Gd_xCo_2$ that we report here is classified into type-II ferromagnetic MPB (type II FM MPB) as shown in Fig. 4(a2). The different transition tendencies at type I FM MPB and

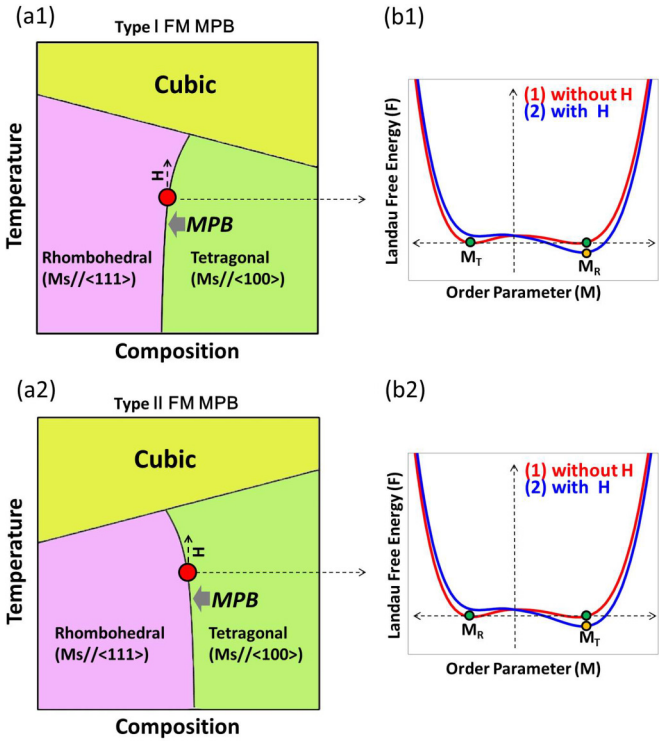

FIG. 4. (Color online) Illustration of (a1) type-I ferromagnetic MPB and (a2) type-II ferromagnetic MPB, and (b1, b2) schematic Landau free energy (F) landscapes at MPB with and without external magnetic field H, with M_R and M_T denoting the order parameter of magnetization in rhombohedral and tetragonal phases, respectively.

type II FM MPB under H are depicted in Figs. 4(b1) and 4(b2). In terms of field-induced response, the common feature of types I and II MPBs is the high ac-field response (magnetic susceptibility) resulted from the weakening of magnetization anisotropy at triple-point-type MPB, similar to that of ferroelectric MPBs [14,15,17,18], and the difference is that type I FM MPB yields large magnetostriction while type II FM MPB yields small magnetostriction. While type I FM MPB materials are promising for devices desiring high magnetostrictive property, type II FM MPB materials might be considered in the future for magnetic recording devices (large susceptibility and small magnetostriction).

Last but not least, attention should be paid to the fact that the symmetry-dependent magnetostriction curves as depicted in Fig. 3 have not been discovered in ferroelectric systems. Ferroelectric MPB composition generally exhibits V-shaped positive electrostriction due to positive lattice distortions in both end member compounds [6,16]. Thus in contrast to the two types of MPBs in ferromagnets, only one type of ferroelectric MPB (PZT, PMN-PT, PZN-PT, BZTBCT, etc.) has been discovered by now [3–6,15,16].

In conclusion, we report a ferromagnetic MPB system $Tb_{1-x}Gd_xCo_2$. Compared to the well-known enhancement effect of MPB on field-induced strain behaviors [6,14–16], $Tb_{1-x}Gd_xCo_2$ shows the inverse effect—magnetostriction value reaches to the minimum at its MPB composition $Tb_{0.1}Gd_{0.9}Co_2$. Such a difference is suggested to arise from the degree of magnetic ordering of compounds forming the MPB systems. Based on our study, we classify $Tb_{1-x}Dy_xCo_2$ (also Terfenol-D [29]) as a type I FM MPB system and the newly discovered $Tb_{1-x}Gd_xCo_2$ as a type II FM MPB system. As far as we know, $Tb_{1-x}Gd_xCo_2$ is the first discovered type II FM MPB (with magnetostriction being not enhanced but weakened at MPB) material. Our work may shed light on designing new magnetoresponsive materials that requires a working state of high susceptibility and low strain, and may also help understand the previously coined "spin reorientation transition" (SRT) involved systems [14,30,31]. Of course, as for the deeper origin of the formation of the two types FM MPBs, it awaits more detailed study.

The authors are grateful to Dr. Zhen Zhang (Iowa State University, US) and MMRC members for helpful discussions. This work was supported by the National Basic Research Program of China (Grant No. 2012CB619401), Kakenhi of JSPS (X. Ren), and the National Natural Science Foundation of China (Grants No. 51222104 and No. 51371134).

[1] V. K. Wadhawan, *Introduction to Ferroic Materials* (Gordon and Breach, Amsterdam, 2000).
[2] R. Newnham, Acta Crystallogr. Sect. A **54**, 729 (1998).
[3] B. Jaffe, W. R. Cook, and H. Jaffe, *Piezoelectric Ceramics* (Academic, New York, 1971).
[4] S. Choi, T. Shrout, S. Jang, and A. Bhalla, Mater. Lett. **8**, 253 (1989).
[5] J. Kuwata, K. Uchino, and S. Nomura, Ferroelectrics **37**, 579 (1981).
[6] W. Liu and X. Ren, Phys. Rev. Lett. **103**, 257602 (2009).
[7] K. A. Schonau, L. A. Schmitt, M. Knapp, H. Fuess, Rudiger-A. Eichel, H. Kungl, and M. J. Hoffmann, Phys. Rev. B **75**, 184117 (2007).
[8] R. Guo, L. E. Cross, S. E. Park, B. Noheda, D. E. Cox, and G. Shirane, Phys. Rev. Lett. **84**, 5423 (2000).
[9] D. Damjanovic, N. Klein, L. Jin, and V. Porokhonskyy, Functional Mater. Lett. **03**, 5 (2010).
[10] J. Kreisel, B. Noheda, and B. Dkhil, Phase Transitions **82**, 633 (2009).
[11] T. Shrout and S. Zhang, J. Electroceram. **19**, 113 (2007).
[12] Y. Saito, H. Takao, T. Tani, T. Nonoyama, K. Takatori, T. Homma, T. Nagaya, and M. Nakamura, Nature (London) **432**, 84 (2004).
[13] A. S. Bhalla, R. Guo, and E. F. Alberta, Mater. Lett. **54**, 264 (2002).
[14] S. Yang, H. Bao, C. Zhou, Y. Wang, X. Ren, Y. Matsushita, Y. Katsuya, M. Tanaka, K. Kobayashi, X. Song, and J. Gao, Phys. Rev. Lett. **104**, 197201 (2010).
[15] C. Zhou, W. Liu, D. Xue, X. Ren, H. Bao, J. Gao, and L. Zhang, Appl. Phys. Lett. **100**, 222910 (2012).

[16] D. Xue, Y. Zhou, H. Bao, J. Gao, C. Zhou, and X. Ren, Appl. Phys. Lett. **99**, 122901 (2011).
[17] M. Porta and T. Lookman, Phys. Rev. B **83**, 174108 (2011).
[18] J. G. A. Rossetti, A. G. Khachaturyan, G. Akcay, and Y. Ni, J. Appl. Phys. **103**, 114113 (2008).
[19] D. Gignoux, F. Givord, and R. Lemaire, Phys. Rev. B **12**, 3878 (1975).
[20] D. Gignoux, F. Givord, R. P. D. L. Bathie, and F. Sayetat, J. Phys. F **9**, 763 (1979).
[21] S. Yang and X. Ren, Phys. Rev. B **77**, 014407 (2008).
[22] A. E. Clark and M. Wun-Fogle, Proc. SPIE **4699**, 421 (2002).
[23] A. E. Clark, in *Power Sonic and Ultrasonic Transducers Design*, edited by B. Hamonic and J. Decarpigny (Springer, Berlin, 1988), pp. 43–99, Chap. 6.
[24] D. Damjanovic, Appl. Phys. Lett. **97**, 062906 (2010).
[25] R. E. Newnham, *Properties of Materials: Anisotropy, Symmetry, Structure* (Oxford University Press, New York, 2004).
[26] S. C. Busbridge and A. R. Piercy, J. Appl. Phys. **73**, 5354 (1993).
[27] K. A. J. Gschneidner, L. Eyring, and G. H. Lander, *Handbook on the Physics and Chemistry of Rare Earths: Volume 32* (North-Holland, Amsterdam, 2001).
[28] C. Zhou, H. Bao, S. Yang, and X. Ren (unpublished).
[29] R. Bergstrom, M. Wuttig, J. Cullen, P. Zavalij, R. Briber, C. Dennis, V. O. Garlea, and M. Laver, Phys. Rev. Lett. **111**, 017203 (2013).
[30] U. Atzmony, M. P. Dariel, E. R. Bauminger, D. Lebenbaum, I. Nowik, and S. Ofer, Phys. Rev. B **7**, 4220 (1973).
[31] U. Atzmony and M. P. Dariel, Phys. Rev. B **13**, 4006 (1976).